ELSEVIER

Composites Science and Technology 59 (1999) 903–910

COMPOSITES SCIENCE AND TECHNOLOGY

An experimental investigation of delamination buckling and postbuckling of composite laminates

Haozhong Gu[1], Aditi Chattopadhyay*,[2]

Department of Mechanical and Aerospace Engineering, Arizona State University, Tempe, AZ 85287-6106, USA

Received 1 December 1997; received in revised form 24 March 1998; accepted 20 July 1998

Abstract

The mechanics and mechanisms of delamination buckling and postbuckling of composites have been studied. Compression tests were carried out on HYE-3574 OH graphite/epoxy composites with built-in delaminations in order to evaluate the critical load and the actual postbuckling load-carrying capacity. The variation in structural configurations, such as ply stacking sequence and the location and the length of the delamination, were considered. It is observed that, in general, composite laminates can retain their load-bearing capacity by carrying higher loads after buckling. For particular cases, the ultimate load is found to be as high as three times the critical load. The delamination buckling mode is found to be closely related to the location and the length of the delamination. Excellent agreement is observed between the experimental values of critical load and those predicted by the previously developed new higher-order theory. Good comparisons are also presented for the initial postbuckling behavior.

1. Introduction

Delamination has been a subject of major concern in engineering applications of composite laminates because of the associated problems of structural integrity and stability, reduction in load-bearing capacity, stiffness degradation and fracture. The mechanics and mechanisms of compressive deformation and failure in delaminated composites have not been fully understood owing to the complexities involved.

Most delamination related studies have primarily focused on the formulation of analytical solutions for the prediction of the buckling load and postbuckling behavior [1–7]. Among the few experimental studies that have been reported, Wang et al. [8] conducted compression tests of delaminated short-fiber composite plates and observed the fundamental characteristics of compressive buckling and crack stability behavior which is unique to delaminated short-fiber composites. Kardomateas [9] focused on postbuckling behavior under large applied displacements and reported some experimental results on the macroscopic behavior of thin delaminations in delaminated Kevlar/epoxy laminates. Nilsson et al. [10] performed an experimental investigation of buckling-induced delamination growth. Suemasu et al. [11] studied the effects of circular and multiple delaminations on the compressive buckling and failure load. They observed that although the failure strength depended on the toughness of the matrix resin, the buckling loads were unaffected by the toughness of the resin. However, these experiments either focused on the critical load or were performed by using very thin or unidirectional composite specimens. Comprehensive information on issues such as the effect of composite lay-up, delamination location and delamination length on delamination postbuckling behavior is still not available. Because of the lack of available and useful experimental data, the results of a detailed experimental investigation are reported in this paper to study the behavior of delamination buckling and postbuckling in composites. The results are used to establish the accuracy of a developed analytical model. Details of the experimental procedure and the results are outlined in this paper.

2. Material and specimen preparation

The material used in all specimens was HYE-3574 OH graphite/epoxy with a nominal ply thickness of approximatel 0.153 mm (0.006 in.). The properties of

* Corresponding author. Tel.: 001 602 965 9342; fax: 001 602 965 1384; e-mail: in%"aditi@asu.edu".

[1] Postdoctoral Fellow, Member AIAA, ASME.

[2] Professor, Associate Fellow AIAA, Member AHS, ASME, SPIE.

0266-3538/99/$ - see front matter
PII: S0266-3538(98)00130-4

the material measured after curing from strain-gauged unidirectional coupons are presented in Table 1. The specimens were constructed to represent variations in: (a) ply stacking sequence, (b) delamination positions and (c) delamination length. Therefore, their effects on delamination buckling and postbuckling could be studied. The length and the width of all specimens were 28 mm × 5.1 mm (11 in. × 2 in.) with a thickness (h) of 5.1 mm (0.201 in.). Three types of flat-plate test specimens, denoted A, B and C with single centered delamination (Figs. 1 and 2) were used in the experiments. The specimens A were constructed by using the ply stacking sequence $[0°/90°/0°]_{12}$ with a mid-plane delamination. For specimen A, six different delamination lengths were studied (A1–A6, see Table 2) to investigate the effects of delamination length on delamination buckling. The specimens B contained a near-surface delamination at a distance (h_1) of 1.33 mm (0.0525 in.) from the surface. The ply stacking sequence of the specimen C were $[-45°/45°]_{9S}$ with a near-surface delamination at a distance (h_1) of 1.7 mm (0.067 in.) from the surface. Four different delamination lengths were also studied using specimens B and C (B1–B4 and C1–C4, see Table 2). Experiments were conducted by using three specimens in each of these categories. Several ply lay-ups selected in manufacturing the specimens represent commonly used arrangements in the industry. The lay-ups were also selected to study the effects of stacking sequence variation on delamination buckling and postbuckling of composite laminates.

In each specimen, the delamination was introduced through double sheets of 0.051 mm (0.002 in.) thick Teflon strips placed at the ply interface through the width (Fig. 1). The specimens were cured by using the modified C-6 cure cycle in an autoclave under 0.7 Mpa (100 psi) pressure. The following cure cycle was used: (a) heat at 1–2°C/min (2–3°F/min) up to 127° ± 6°C (260° ± 10°F), (b) hold at that temperature for 2 h and (c) cool under the pressure 2–3°C/min (3–5°F/min) to 65.6°C (150°F). Since the curing process affects the final dimensions, the exact plate thickness (h) of the specimen was measured with a micrometer after curing and was found to be 5.1 mm (0.201 in.).

A simple coupon configuration is desirable for practical evaluation of material and laminate load-carrying capacity. A problem associated with flat-plate compression test specimens is the possibility of material failure rather than the desired delamination buckling under compressive loads. This problem was eliminated by selecting plate dimensions whose critical buckling stress is much lower than the ultimate strength of the material.

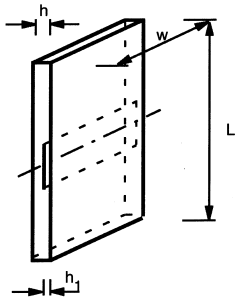

Fig. 1. Compression test specimens.

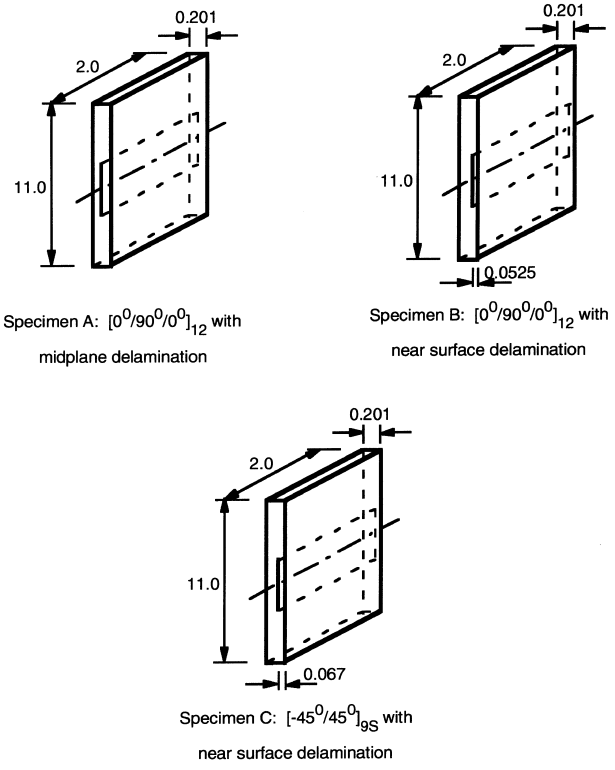

Fig. 2. Geometries of specimens.

Table 1
Material properties for HYE-3574 OH graphite/epoxy fabric

Material property	Value
Longitudinal Young's modulus, E_L (Gpa)	100.7
Transverse Young's modulus, E_T (Gpa)	8.27
Poisson's ratio, υ_{LT}	0.25
Poisson's ratio, υ_{TT}	0.25
Shear modulus, G_{LT} (Gpa)	3.45
Shear modulus, G_{TT} (Gpa)	2.41

Table 2
Specimen specification

Specimen number	A1	A2	A3	A4	A5	A6	B1
Delamination length (in.)	1.5	2.5	3.5	4.5	6.0	7.5	1.5
Specimen number	B2	B3	B4	C1	C2	C3	C4
Delamination length (in.)	2.5	3.0	4.5	1.5	3.0	4.5	6.0

3. Experimental procedure

All tests were conducted using a 50-kip Instron testing equipment (Fig. 3) and a data acquisition system, which consists of a MTS Test Star II controller, a LVDT controller and a 486 IBM PC running test software entitled Test Star version 2.0c. The test data were digitally recorded and pre- and post-test photographs were taken. The experimental setup for the compression tests is shown in Figs. 3 and 4. A total of 42 specimens were tested. The specimen was clamped at two ends with specially designed fixtures (Fig. 4). The specimen slides into these fixtures and therefore no bending is introduced by tightening the end. The opening of the fixture is adjustable so that slight changes in thickness do not affect the effectiveness of the fixed-end conditions of the specimen. Moreover, the alignment of the specimen could be adjusted by inserting metal sheets of various thicknesses into the opening of the fixture. To ensure truly fixed boundary conditions, 25 mm (1 in.) at the edge of the specimen, along the length, was restrained by each fixture. The effective length between two end fixtures was therefore 23 mm (9 in.) for all specimens.

The tests were carried out on stroke control with a rate of about 0.35 mm/min (0.012 in./min). The load and axial displacement data were digitally recorded. Two linear variable displacement transducers were used to measure the midpoint deflections of the delaminated layers and the sublaminates. This determined the magnitude of delamination opening. The delamination growth could be captured by the sudden change in the compressive load and the corresponding displacements. The specimen was unloaded once visible material failure had occurred.

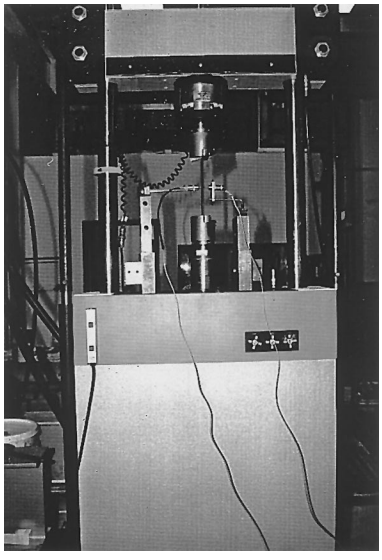

Fig. 3. Mechanical test equipment.

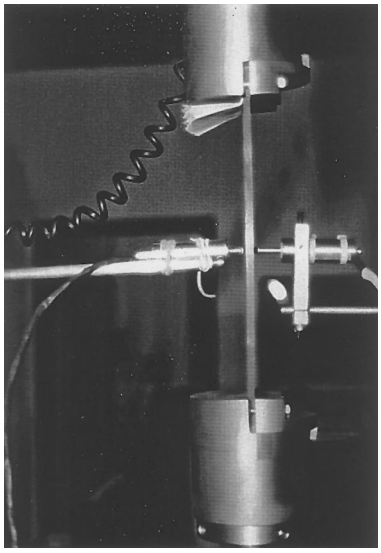

Fig. 4. Compression test setup.

4. Observations

The deformation history of all specimen configurations has been analyzed by studying the variation of compressive stress with axial displacement and the variation of mid-point deflection with compressive stress. Snapshots of buckling and postbuckling behavior, in certain instances, are presented to explain the physical phenomena occurring during the test.

Fig. 5(a) and (b) present the results obtained with specimens A with various delamination lengths. In Fig. 5(a), point B corresponds to the buckling point of the laminate or the delaminated layer and point U represents the ultimate load sustained by the specimen. Points D and G are used to denote the region of the sudden drop in load phase due to delamination growth or material damage. The quantity δ_L is the axial length shortening during the compressive loading procedure and δ_T is the mid-point deflection of the laminate. The buckling point can be determined by examining the transverse deflection in the load-deflection curve (Fig. 4(a)). Once transverse deflection occurs, buckling of the delaminated layer or the laminate takes place. In all four cases presented (Fig. 5(a) and (b)), quite good linear relationships between the applied compressive stress and the axial displacement are observed during the prebuckling state. However, the non-linearity of relationships is noticed during postbuckling deformation. As seen from Fig. 5(a) and (b), both the critical stress and the ultimate stress reduces as the delamination length increases. The ratio of the ultimate stress to the critical stress increases with the increase in the delamination length. This observation indicates that delamination has more effect on the critical load than on the load-carrying capacity. The sudden drops in load are caused by the sudden material damage near the fixtures

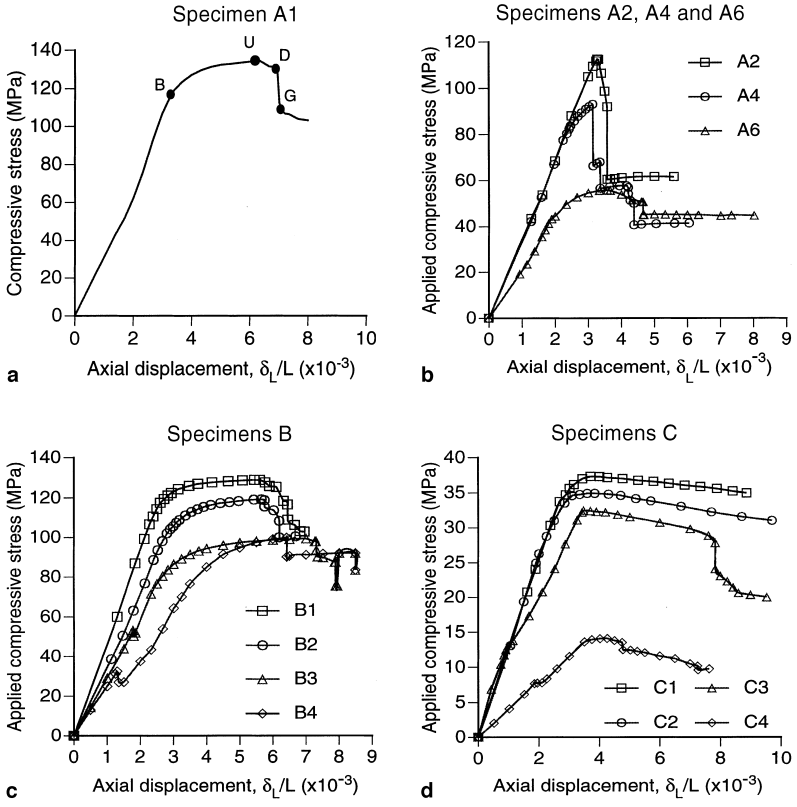

Fig. 5. Postbuckling path for test specimens. (a) Specimen A1; (b) Specimens A2, A4 and A6; (c) Specimens B; (d) Specimens C.

in cases A1 and A2 (short delamination length). In cases A4 and A6 (intermediate and long delamination lengths), they are caused by the sudden delamination growth. Only global buckling mode (no opening at the delamination interface between the delaminated layer and the sublaminate) is observed in these cases (Fig. 6(a) and Fig. 7) since a mid-plane delamination indicates a thicker delaminated layer.

Fig. 5(c) shows the buckling and postbuckling history for specimens B with various delamination lengths. In these four cases, the delamination location is near the surface, which indicates that the delamination layer is relatively thin. Therefore, the critical stress, dominated by the local buckling of the thin delaminated layer, becomes much smaller than the ultimate stress in cases B3 and B4 for relatively long delamination lengths. After the buckling of the delaminated layer, the relatively thick sublaminate still retains its load-carrying capacity. Therefore, the plate as a whole is capable of carrying a much higher ultimate load. For example, the ultimate load obtained in specimen B4 is as high as three times its critical load. Two regions of sudden drop in load, caused by delamination growth, are observed in cases B3 and B4. Only one region of sudden drop in load is observed in cases B1 and B2, which is caused by material damage. The local and mixed (combined local with global modes) delamination buckling modes (opening modes) are observed in cases B3 and B4 (Fig. 6(b)) because of their thinner delaminated layers and longer delamination lengths. Fig. 8 presents a snapshot taken at the instance of the initial delamination opening.

Experimental results are also presented in Fig. 5(d) for angle-ply composites with near-surface delamination (specimens C1–C4). Again, much higher ultimate stress compared to the critical stress is obtained and local and mixed delamination buckling modes (opening mode) is observed in cases C3 and C4. In all of four cases, the sudden drop in load phases are caused by the delamination growth. The delaminated layer and the sublaminate deflect in opposite directions over the entire postbuckling path (Fig. 6(c)), which is different from what is observed in specimen B (Fig. 6(b)). This is because of the relatively thicker delaminated layer in this case (the delamination is located at a distance of 1.7 mm (0.067 in.) from the surface for specimens C rather than 1.33 mm (0.0525 in.) for specimens D). Fig. 9 shows a snapshot taken during the tests when delamination was separated.

5. New higher-order theory

The results of this experimental investigation are used to validate the previously developed new higher-order theory for delamination buckling and postbuckling analysis by Chattopadhyay and Gu [1]. A brief outline of the theory is presented here. A higher-order through-thickness

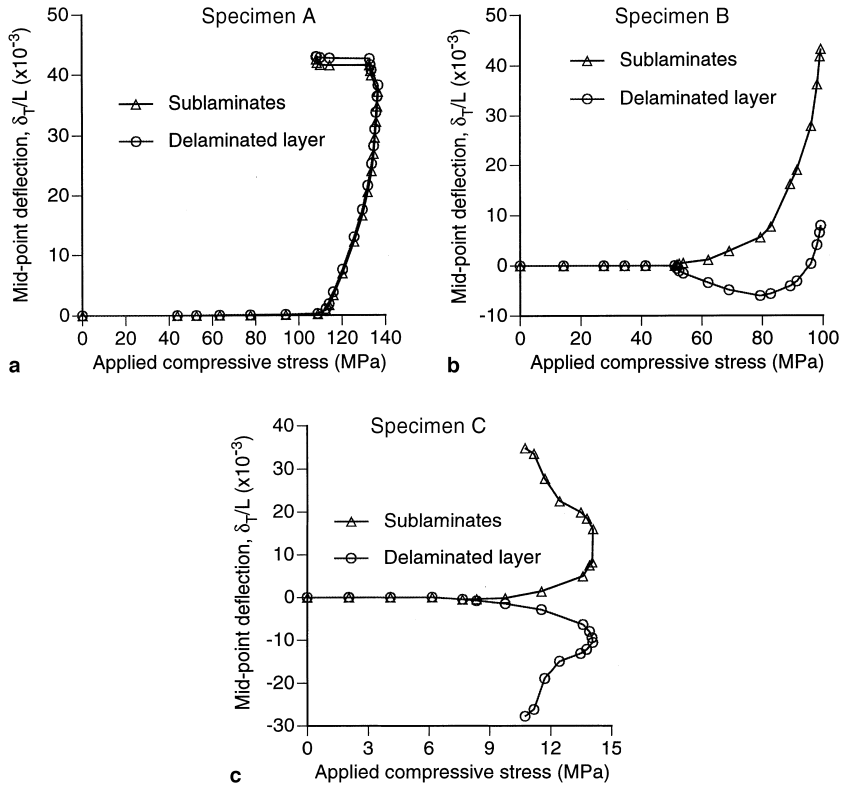

Fig. 6. Variations of mid-point deflection with compressive stress. (a) Specimens A; (b) Specimens B; (c) Specimens C.

displacement field is used in the theory to describe the transverse shear deformations in an effort to capture the transverse shear effects in delaminated composites. The displacement field is described by three groups below.

$$
\begin{aligned}
u_1(x,y,z) &= \sum_{j=0}^{N} z^j\{U_{0j}(x,y) + [1 - H(z^*)]U_{1j}(x,y) \\
&\quad + H(z^*)U_{2j}(x,y)\}, \\
u_2(x,y,z) &= \sum_{j=0}^{N} z^j\{V_{0j}(x,y) + [1 - H(z^*)]V_{1j}(x,y) \\
&\quad + H(z^*)V_{2j}(x,y)\}, \\
u_3(x,y,z) &= W_0(x,y) + [1 - H(z^*)]W_1(x,y) \\
&\quad + H(z^*)W_2(x,y),
\end{aligned}
\tag{1}
$$

where, (u_1, u_2, u_3) are the displacements at an arbitrary point (x, y, z) on the plate, (U_{00}, V_{00}, W_0) denote the displacements defined on the midplane of the plate, (U_{0j}, V_{0j}, $j = 1, 2, \ldots, N$) are the jth order transverse shear correction terms. Heaviside step function $H(z^*)$ is used to provide the jumps in displacement between the sublaminate and the delaminated layer at delamination interface, which are given by (U_{1j}, V_{1j}) and (U_{2j}, V_{2j}), $j = 0, 1, \ldots, N$, respectively. Therefore, this displacement field is capable of describing the separation and slipping conditions at delamination interface. Further, by properly defining the functions (U_{1j}, V_{1j}) and (U_{2j}, V_{2j}), $j = 0, 1, \ldots, N$, the exact continuity conditions can be satisfied automatically at delaminated and undelaminated interfaces. These continuity conditions are generally applied approximately in other approaches [2–4]. It is also possible for the displacement field to provide traction-free conditions at delamination interface due to the independence of the displacements on adjacent layers at the delamination interface. Here, $N = 4$ is

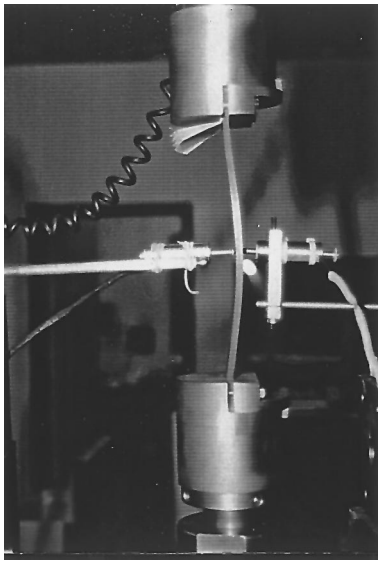

Fig. 7. Buckling modes in mid-plane delamination cases.

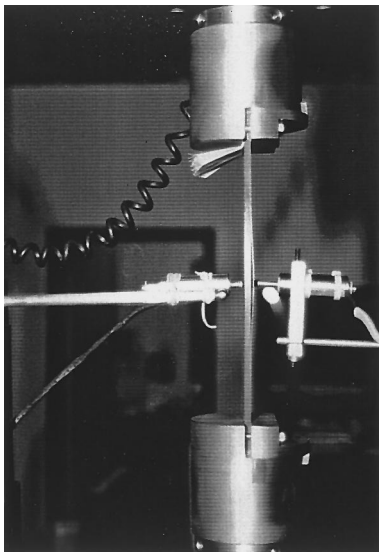

Fig. 8. Buckling modes in near-surface delamination cases.

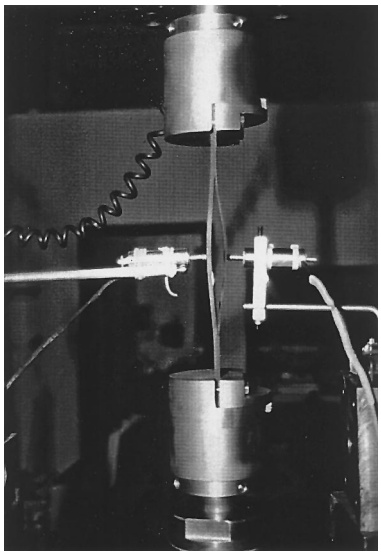

Fig. 9. Buckling modes in angle-ply composites.

used to formulate the displacement field. The specific forms of the higher order terms, U_{im} and V_{im} ($m=3,4$), are derived by applying traction-free boundary conditions at all free surfaces.

$$U_{04} = -\frac{2}{h^2}U_{02},$$

$$V_{04} = -\frac{2}{h^2}V_{02},$$

$$U_{13} = -\frac{4}{3h^2\alpha^2}\left[(1-\alpha)(U_{01}+W_{0,x}) + h\alpha(1-\alpha)(U_{02}+U_{12}) + (1-\alpha+\alpha^2)(U_{11}+W_{1,x})\right],$$

$$V_{13} = -\frac{4}{3h^2\alpha^2}\left[(1-\alpha)(V_{01}+W_{0,y}) + h\alpha(1-\alpha)(V_{02}+V_{12}) + (1-\alpha+\alpha^2)(V_{11}+W_{1,y})\right],$$

$$U_{14} = -\frac{2(1-\alpha)}{h^3\alpha^2}\left[U_{01}+W_{0,x}+h\alpha\left(\frac{U_{12}}{1-\alpha}+U_{02}\right) + U_{11}+W_{1,x}\right],$$

$$V_{14} = -\frac{2(1-\alpha)}{h^3\alpha^2}\left[V_{01}+W_{0,y}+h\alpha\left(\frac{V_{12}}{1-\alpha}+V_{02}\right) + V_{11}+W_{1,y}\right],$$

$$U_{23} = -\frac{4}{3h^2\alpha^2}\left[(1+\alpha)(U_{01}+W_{0,x}) + h\alpha(1+\alpha)(U_{02}+U_{22}) + (1+\alpha+\alpha^2)(U_{21}+W_{1,x})\right],$$

$$V_{23} = -\frac{4}{3h^2\alpha^2}\left[(1+\alpha)(V_{01}+W_{0,y}) + h\alpha(1+\alpha)(V_{02}+V_{22}) + (1+\alpha+\alpha^2)(V_{21}+W_{1,y})\right],$$

$$U_{24} = \frac{2(1+\alpha)}{h^3\alpha^2}\left[U_{01}+W_{0,x}+h\alpha\left(\frac{U_{22}}{1+\alpha}+U_{02}\right) + U_{21}+W_{2,x}\right],$$

$$V_{24} = \frac{2(1+\alpha)}{h^3\alpha^2}\left[V_{01}+W_{0,y}+h\alpha\left(\frac{V_{22}}{1-\alpha}+V_{02}\right) + V_{21}+W_{2,y}\right], \tag{2}$$

where

$$\alpha = 2z^*/h. \tag{3}$$

Substituting Eq. (2) into Eq. (1), the refined displacement field is obtained [1]. By using variational principle, the governing equations and the associated boundary conditions are derived for the delamination buckling and postbuckling analysis. In general, the nonlinear governing equations for delamination postbuckling can be written as

$$(\mathbf{K}_{\mathrm{L}} + \mathbf{K}_{\mathrm{N}})\mathbf{a} = \mathbf{f}, \tag{4}$$

where, $\mathbf{K}_{\mathrm{L}}$ and $\mathbf{K}_{\mathrm{N}}$ are the linear and the nonlinear components of the direct stiffness matrix, respectively, $\mathbf{a}$ is generalized displacement vector and $\mathbf{f}$ is the load vector. The linear buckling equations are simplified as

$$(\mathbf{K}_{\mathrm{L}} + \lambda\mathbf{K}_{\mathrm{G}})\mathbf{a} = 0 \tag{5}$$

in which, $\mathbf{K}_{\mathrm{G}}$ is the geometric stiffness matrix and λ is the critical load parameter.

6. Correlations

The experimental results are now used to validate the solution provided by the new higher-order theory. Fig. 10(a) shows a comparison of critical stresses obtained from the experimental results with those obtained using both the classical laminate theory and the new higher-order theory for cross-ply composites with mid-plane

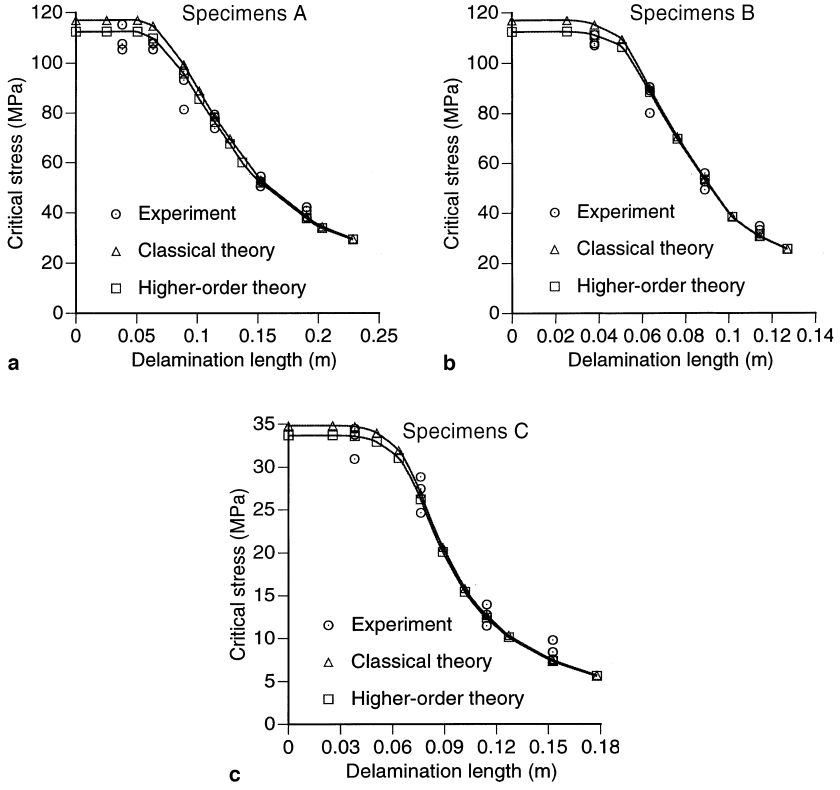

Fig. 10. Comparison of critical stress obtained form experiments and theories. (a) Specimens A; (b) Specimens B; (c) Specimens C.

delamination (specimens A). The circled data points represent the 18 individual specimens whose buckling loads are determined from the load deflection curves (Fig. 6). Very good agreement is observed between results of the new higher-order theory and experiments. Although the plate specimens are relatively thin, with length to thickness ratio (L/h) of 44.8, a noticeable deviation is observed from the results computed using the classical laminate theory compared to those obtained from both the new higher-order theory and experimental data. The deviation is more significant in plates with short delamination and is reduced in plates with longer delamination due to the changes in delamination buckling modes [12,13]. Comparisons for cross-ply composites with near-surface delamination (specimens B) and angle-ply composites with near-surface delamination (specimens C) are also presented in Fig. 10(b) and (c), respectively. Once again, the classical laminate theory over-predicts the critical stress in these two cases. For angle-ply composites, since the transverse shear effect reduces with reduction in the ratio of spanwise Young's modulus to transverse shear modulus (E_x/G_{xz}) compared to cross-ply composites, the deviation becomes smaller. Results obtained from the new higher-order theory also correlate very well with experimental data in both cases. These agreements indicate that the new higher-order theory provides accurate critical load estimates of delamination buckling of composites.

Comparisons are also made for the initial postbuckling behavior between results from the experiments and the new higher-order theory. Fig. 11(a) and (b) present the stress-deflection curves for cross-ply composites with both mid-plane delamination (specimen A1) and near-surface delamination (specimen B3). The circled data points in Fig. 11(a) represent the results obtained from one of the A1 specimens. Less than 10% deviations are observed between the experimental results and the solutions from the new higher-order theory in this case. In Fig. 11(b), the quantities w_{se} and w_{de} refer to the experimentally determined values of the mid-point deflections of the sublaminate and the delaminated layer, respectively. The quantities w_{sh} and w_{dh} represents the mid-point deflections of the sublaminate and the delaminated layer obtained from the new higher-order theory. Again, the solutions from the new higher-order theory correlate quite well with the experimental results. These correlations indicate that the new higher-order theory is reliable in predicting the delamination postbuckling behavior of composites. Since the later stage of the postbuckling behavior, recorded during the experiments, are coupled with other structural and material damage, it cannot be used to predict the ideal delamination postbuckling behavior.

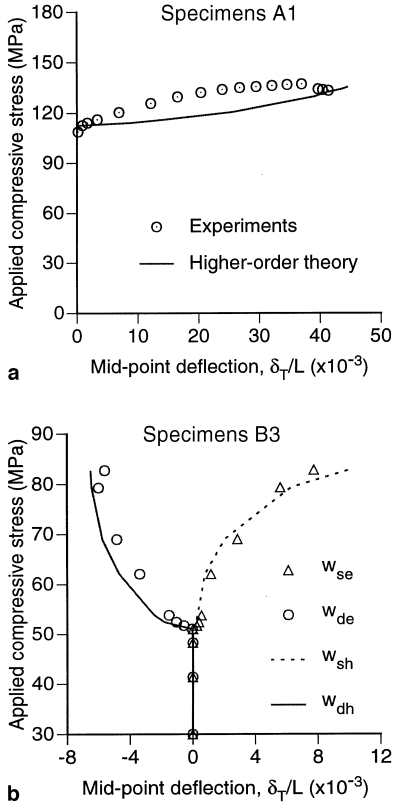

Fig. 11. Comparison of postbuckling behaviors; experiment and higher-order theory. (a) Specimen A1; (b) Specimen B3.

7. Concluding remarks

A detailed experimental investigation was performed to study the behavior of delamination buckling and postbuckling. The flat-plate specimens were made up of graphite/epoxy. Various delaminations of different sizes and locations were introduced through double sheets of Teflon strips placed in the interface of the delamination through the width. The test results are used to validate the analytical results obtained using a new higher-order laminate theory. The following important observations were made:

1. The experimental investigation provides a comprehensive data base, on delamination buckling and postbuckling behavior of composites, for analytical correlations.
2. The experimental results validate the new higher-order theory of delaminated composite plates for both buckling and postbuckling analysis.
3. The observations on buckling mode made form the experimental results agree with those obtained through analytical investigations.
4. In general, composite laminates can still retain their load bearing capacity after buckling. For composites with thinner and longer delamination, the ultimate load obtained through the experiments is as high as three times their critical load.

Acknowledgements

The research was supported by the US Army Research Office, Grant No. DAAH04-93-G-0043, Technical monitor, Dr. Gary Anderson. The authors would also like to acknowledge Dr. Ken Lou and Mr. Tony Cook at Simula Inc. for their support in preparing the test specimens and Dr. Barzin Mobasher and Mr. Calvin Young for their assistance in running experiments.

References

[1] Chattopadhyay A, Gu H. A new higher-order plate theory in modeling delamination buckling of composite laminates. AIAA J 1994;32(8):1709–16.
[2] Chai H, Babcock CD, Krauss WG. One dimensional modeling of failure in delaminated laminates. Int J Solid Structures 1981;17(11):1069–83.
[3] Sallam S, Simitses GJ. Delamination buckling and growth of flat, cross-ply laminates. Compos Struct 1985;4:361–81.
[4] Kardomateas GA, Schmueser DW. Buckling and postbuckling of delaminated composites under compressive loads including transverse shear effects. AIAA J 1988;26(3):337–43.
[5] Chen HP. Shear deformation theory for compressive delamination buckling and growth. AIAA J 1991;29(5):813–19.
[6] Barbero EJ, Reddy JN. Modeling of delamination in composite laminates using a layer-wise plate theory. Int J Solid Structures 1991;28(3):373–88.
[7] Kardomateas GA. The Initial Postbuckling and Growth Behavior of Internal Delaminations in Composite Plates. J Applied Mechanics 1993;60:901–10.
[8] Wang SS, Zahlan NM, Suemasu H. Compressive stability of delaminated random short-fiber composites – Part II. Experimental and analytical Results. Journal of Composite Materials 1985;19:317–33.
[9] Kardomateas GA. Postbuckling characteristics in delaminated Kevlar/epoxy laminates: an experimental study. J Compos Technol & Research 1990;12(2):85–90.
[10] Nilsson KF, et al. A theoretical and experimental investigation of buckling induced delamination growth 1993;J. Mech. Phys. Solid 1993;41(4):783–807.
[11] Suemasu H, Kumagai T, Gozu K. Compressive behavior of rectangular composite laminates with multiple circular delaminations. Proceedings of 37th AIAA/ASME/ASCE/AHS/ASC Structures, Structural Dynamics and Materials Conference, April 15–17, 1996, Salt Lake City, UT, 2252–8.
[12] Gu H, Chattopadhyay A. Elasticity solution for delamination buckling of plates, Proceedings of 37th Structures, Structural Dynamics and Materials Conference, Apr. 15–17, 1996, Salt Lake City, UT, 2543–51; AIAA J, (in press).
[13] Gu H, Chattopadhyay A. Three dimensional elasticity approach for delamination buckling of composite plates, Proceedings of 38th Structures, Structural Dynamics and Materials Conference, April 7–9, 1997, Kissimmee, Florida, 2629–38.